Interpretation of the Laser-Induced Emissions for flame-synthesized TiO 2 nanoparticles

J Yi, Christopher Betrancourt, Nasser Darabiha, Benedetta Franzelli

Interpretation of the Laser-Induced Emissions for flame-synthesized TiO_2 nanoparticles

J. Yi[1], C. Betrancourt*[1], N. Darabiha[1], and B. Franzelli*[1]

[1]Laboratoire EM2C, CNRS, CentraleSupélec, Université Paris-Saclay, 91190 Gif-sur-Yvette, France

Abstract

Among various techniques for monitoring of particle formation in flames, laser-induced incandescence (LII) has generally been developed for soot particles. Recent works have shown the feasibility of LII for flame-synthesized TiO_2. However, extensive work is still needed to use this technique to quantitatively characterize TiO_2 production in flames. In this work, first attempts towards the characterization of TiO_2 synthesis in flames are provided in terms of normalized volume fraction and primary particle diameter. To achieve this, TiO_2 nanoparticles are generated in a laminar diffusion flame of argon-diluted hydrogen and air with pre-vaporized Ti-precursor. A 355 nm laser is used to irradiate the flame-generated particles, and spectral, temporal and spatial measurements are performed. First, laser-induced emission at prompt is investigated for different laser fluences to identify the operating conditions that ensure the LII-like nature of the measured signals and infer the composition of the produced nanoparticles. Then, it is shown that it is possible to obtain information from the LII signal on the spatial evolution of the normalized volume fraction and the primary particle size.

Introduction

The synthesis of TiO_2 nanoparticles via flame spray pyrolysis has gained significant interest due to its efficiency and versatility in producing high-quality particles with tailored properties [1]. For this, a good understanding of the processes governing nanoparticle production in the flame is required. Among the different available in-situ diagnostics, laser-induced incandescence (LII) has been originally developed to obtain information on the volume fraction and primary particle size of carbonaceous particles [2]. In this work, we aim to extend this approach to the characterization of flame-synthesized TiO_2 nanoparticles.

LII technique has already been applied to various non-soot nanoparticles [3]. Specifically, for TiO_2, LII has been performed for flame synthesis but in the presence of carbon materials [4–7]. Even if very recent work has proven its feasibility for high-purity TiO_2 in a non-reactive environment [8], the interpretation of LII signal in terms of quantitative volume fraction and primary particle size remains challenging for two main reasons. First, laser-induced emission (LIE) can be characterized by signals such as laser-induced fluorescence (LIF), phase-selective laser-induced breakdown spectroscopy (PS-LIBS) and LII as a function of the laser fluence. Second, experimental data on TiO_2 optical properties, specifically the refractive index absorption function $E(m_\lambda)$, present large uncertainties [9, 10] affecting the LII signal interpretation. The objective of this study is to provide first indications on the interpretation of LII signal in terms of the volume fraction and size of TiO_2 nanoparticles in flame synthesis.

This article is organized as follows: first, the experimental set-up used for TiO_2 nanoparticle synthesis is described in Sec. 1. Next, the LIE of flame-synthesized TiO_2 nanoparticles is characterized in Sec. 2. Finally, section 3 introduces the interpretation of the LII signal in terms of volume fraction and particle size.

1 Experimental set-up

The experimental set-up illustrated in Fig.1 is constituted of three parts: laser heating, signal detection, and TiO_2 particle synthesis in laminar coflow flame. In order to induce TiO_2 LIE, the 3rd harmonic of an Nd:YAG laser (Quantel, Q-smart 850) at 10 Hz with a 5 ns width pulse is used. The laser fluence is adjusted through an attenuator that consists of a half-wave plate and two polarizers. A beam profiler (Gentec Beamage) is employed to monitor the energy distribution of the nearly top-hat-shaped laser (not presented here), which is 1:1 relay-imaged at the centerline of the burner.

The induced signal is collected at 90° using a telescope composed of two two-inch achromatic lenses (f1 = 200 mm and f2 = 100 mm). Two notch filters (355 and 532 nm) are used to suppress the laser harmonic signal. The collected signal is then focused on a 365 μm multimode optical fiber (Thorlabs, FG365UEC) leading to the entrance slit of a spectrometer resulting a spectral resolution of 0.17 nm. The signal is imaged at 10 Hz with a gate width of 20 ns at different gate delays using a spectrometer (Princeton Instrument, Spectra Pro HRS-500, f = 500 mm, 150 grooves/mm) coupled with an intensified CCD camera (Princeton Instruments, PI-MAX 4 1024EMB). The detection system is calibrated using a tungsten filament lamp for signal intensity and a mercury lamp for wavelength. The time-resolved LIE signal is measured using a photomultiplier (PMT, HAMAMATSU, R2257) at 640$\pm$10 nm and recorded using an oscilloscope (Lecroy wave surfer 434, 350MHz bandwidth, 2GS/s sampling rate).

At the opposite side of the telescope detector, an intensified camera (Princeton Instruments, PI-MAX 4, 1024i) equipped with a bandpass filter centered at 640

*Corresponding authors: benedetta.franzelli@centralesupelec.fr, christopher.betrancourt@centralesupelec.fr

Proceedings of the European Combustion Meeting 2023

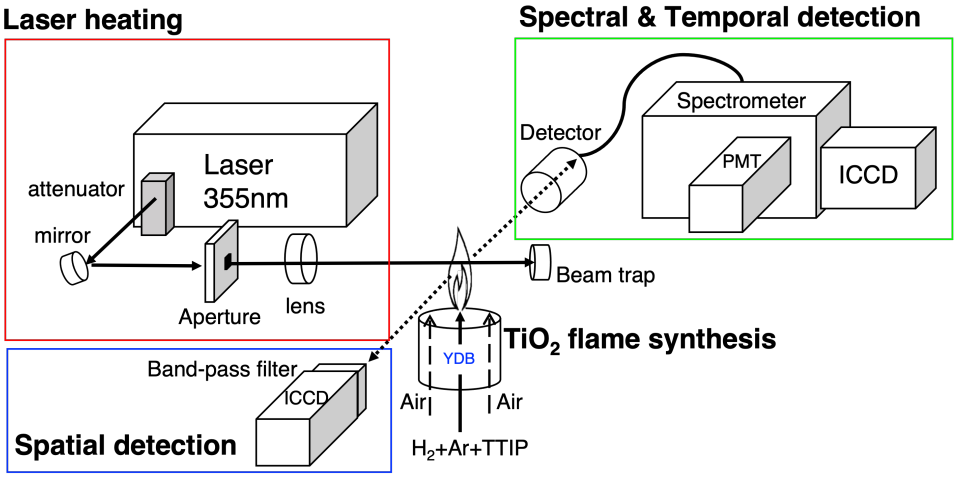

Figure 1: Schematic presentation of the experimental set-up developed to investigate the laser-induced emission from TiO_2 nanoparticle in flame using a pulse YAG laser at 355 nm.

nm $\pm$ 7 nm (Edmund optics, 86995) is placed to study the spatial distribution of the LIE. Signals are recorded in a two-dimensional grid with a width of 8 mm and a height of 1 mm, covering the homogeneous laser top-hat with a height of 0.9 mm. The detection timing is synchronized with the laser peak. The gate width is 20 ns.

To measure at different flame heights, the burner holder is moved using a hydraulic crank with an accuracy of 10 μm in the z-direction of height above the burner (HAB) each 2 mm. Each measurement displayed in this work is corrected from the background.

To synthesize TiO_2 nanoparticles in flame, the design of the Yale diffusion burner (YDB) [11] is used. The burner consists of a central fuel tube (inner diameter D_i= 3.9 mm) surrounded by air coflow (inner diameter D_o = 76 mm). The precursor used to generate TiO_2 nanoparticles is titanium isopropoxide $Ti(OCH(CH_3)_2)_4$ (TTIP, Sigma Aldrich, purity $\geq$ 97.0%) in a pressurized bottle at 6 bar with a N_2. The TTIP mass flow rate is controlled by a Coriolis flowmeter (Bronkhorst, MINI CORI-FLOW, ML120V21-BAD-11-0-S) and introduced through a heated line at 403 K to ensure its vaporization. The TTIP vapor is then mixed with heated H_2-Ar at 353 K And transported to the thermalized burner at 423 K. Finally, at the exit of the burner, the temperature keeps 380 K for the fuel exit in the middle and around 412 K for the coflow air exit. A detailed description of the injection and heating system can be found in [8].

H_2 was chosen as the fuel for synthesizing TiO_2 nanoparticles in order to minimize the presence of carbon species. To increase the stability of the flame, the fuel was mixed with Ar in the fuel tube. In order to prevent hydrolysis during precursor pre-vaporization, the H_2O levels were strictly controlled to be below 0.5 ppm for hydrogen and argon. The operating conditions are presented in Table 1. A typical H_2-Air flame is illustrated in Fig. 2(a). Upon injection of TTIP into the hydrogen flame, a bright, cylindrical area with a diameter of approximately 4.5 mm is observed, as shown in Fig. 2(b). The flame structure is schematically illustrated in Fig. 2(c). This luminous zone indicates the presence of TiO_2 nanoparticles. This zone changes color from orange to white and then has a pale-blue tail. The bright zone is surrounded by a much weaker luminescent flame similar to the hydrogen flame without TTIP.

Fuel				Coflow	
$\dot{m}_{H_2}$	$\dot{m}_{Ar}$	$\dot{m}_{TTIP}$	T_F	$\dot{m}_{air}$	T_C
5.1 g/h	2.3 g/h	0.5 g/h	380 K	7759 g/h	412 K

Table 1: Operating conditions for the preheated hydrogen and precursor (TTIP) coflow flame. The inflow velocity is 1.9 m/s, and the coflow velocity is 0.55 m/s.

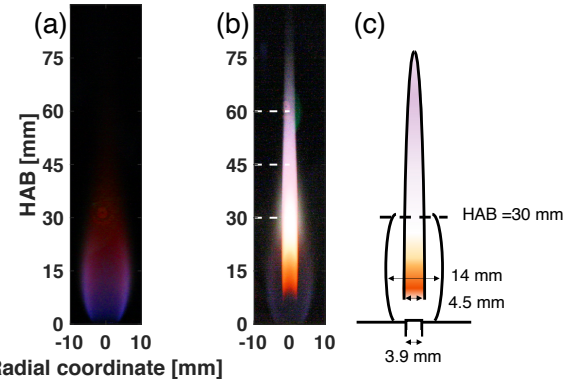

Figure 2: Typical images of the luminosity of H_2/Ar/Air coflow diffusion flames before (a) and after (b) injection of TTIP precursor. The camera exposition is adapted for better visualization for each figure. (c) Schematic illustration of H_2/Ar/Air/TTIP flame.

1.1 Consistency between detection devices

To ensure that the three detection devices are consistent in terms of spectral, temporal and spatial characteristics, their results are compared at a detection wavelength of 640 nm at the centerline of the flame at HAB = 30 mm, corresponding to the most luminous zone. Various time delays were considered. The comparison is illustrated in Fig. 3. The spectral signals have been integrated for the target wavelength range at each detection timing and then normalized by maximum. The same is done for the temporal signals that have been over a duration of 20 ns. For the camera, the signal intensities of all pixels in the equivalent detection volume are added up. Overall, the normalized signals show good agreement between the three detection devices, which guarantees the consistency between the three measurement systems. The

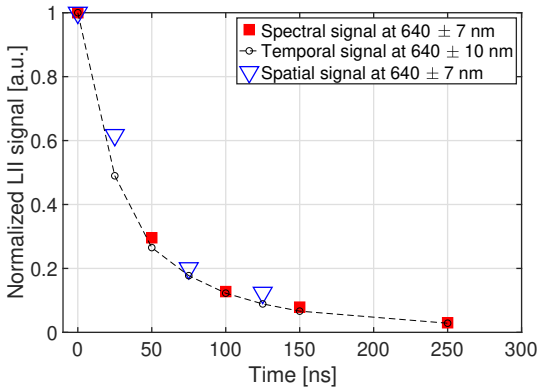

Figure 3: Comparison between data from the three different detection devices for λ_{em} = 640 nm: ICCD camera on the spectrometer (spectral, red square symbol), PMT on the spectrometer (temporal, black round symbol with dashed line) and another ICCD camera (spatial, blue triangle symbol). Measurements were performed at the centerline at HAB=30 mm.

variability at the centerline of the LII measurement has been examined by looking at 7 sets of temporal measurements via PMT in Fig. 4. It is important to notice that the LII measurement data show about a 30 % of standard deviation variation. This is probably due to the fact that TiO_2 production in the flame is not perfectly steady. This indicates that the experimental burner, especially the injection system, requires to be improved in the future. Overall, the intensity, the spatial, and the temporal evolutions of the signal are quite reproducible.

2 Laser-induced emission of flame-synthesized TiO_2

The emission spectra of TiO_2 particles produced by flame at HAB of 30 mm are presented for various laser fluences in Fig. 5. At low fluence levels (F = 0.1 J/cm^2 and F = 0.15 J/cm^2), the emission displays a smooth and broad band of light in the visible range, with no distinct features except for the small peak around 500 nm for F = 0.15 J/cm^2. In contrast, sharp peaks are more noticeable at F = 0.19 J/cm^2 than at F = 0.24 J/cm^2, which suggests that non-thermal interference from LIF

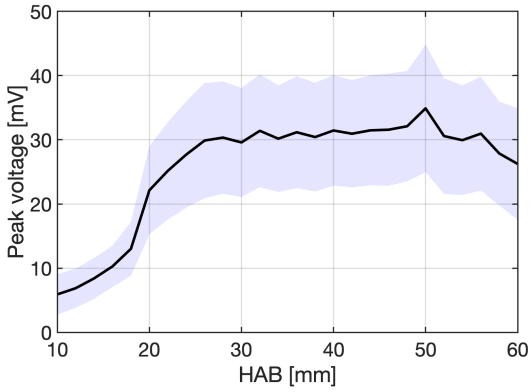

Figure 4: Variability of LII signal intensity from 7 sets of temporal measurements via PMT at prompt along the flame centerline. Standard deviations (σ) are represented by blue area and the averaged values are represented in black lines.

and/or PS-LIBS are present, similarly from what has been observed for TiO_2 nanoparticles in a cold environment [8].

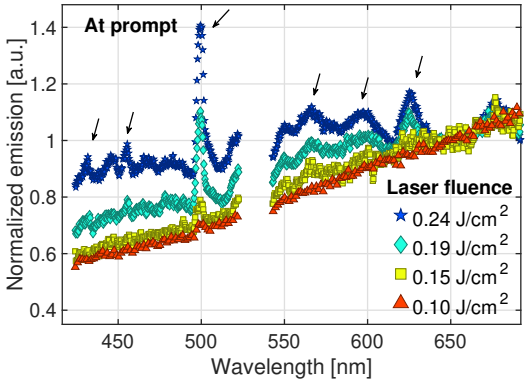

Figure 5: Effect of laser fluence F on LIE spectra at prompt for flame-generated TiO_2 nanoparticles at HAB = 30mm. Spectra are normalized by the value of 650 nm. Ti atomic emissions from NIST [12] are represented by arrows.

In Fig. 6, the LIE spectra of TiO_2 nanoparticles produced by flame at HAB = 30 mm are displayed, for various acquisition delays from the prompt timing at a laser fluence of 0.15 J/cm^2. The emission spectra exhibit a red-shift with increasing time delay, indicating a decrease in temperature as predicted by LII theory. As already mentioned from prompt results, there is a peak emission visible at 500 nm which corresponds to Ti emission [12], and these sharp features vanish quickly with time and are not present for longer wavelength near 640 nm. Therefore, wavelengths longer than 630 nm and low laser fluence range ($\leq$ 0.15 J/cm^2) are proposed to perform LII measurements without the need for any delay times. If higher fluences or smaller wavelengths are considered, a delay should be introduced to acquire the signal suggested by De Iuliis et al. [6, 7].

It is however important to verify that the measured LII signal corresponds to TiO_2 nanoparticles. Indeed,

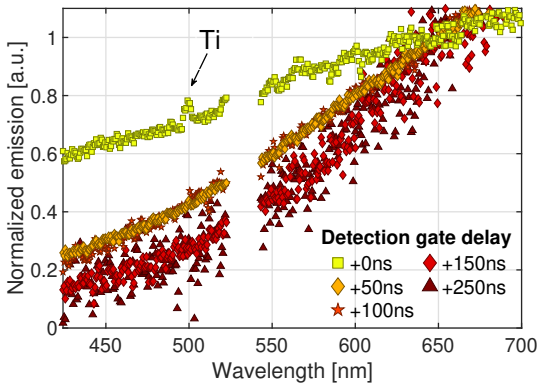

Figure 6: Effect of gate delay (gate width = 20 ns) on emission spectra of LIEs of flame-generated TiO_2 nanoparticles at laser fluence of F = 0.15 J/cm^2. Spectra are normalized with the value of the spectrum at 650 nm.

if carbon materials are found in the flame, it might contribute to the LII signal so that it would be challenging to analyze TiO_2 production. As an example, Ren et al. [13] synthesized a carbon-metal-oxide nanocomposite using C_2H_4 in a counterflow burner. The emission spectrum of carbon-coated TiO_2 nanoparticles showed both the line features from Ti atoms (near 500 nm) and the C_2 emission from the carbonaceous component (near 516 nm), indicating the presence of carbon materials on the surface of TiO_2 particles. Similarly, the C_2 swan bands from the excited carbon species [14] were detected in LIE of TiO_2 nanoparticles synthesized in flames assisted by premixed CH_4/Air flames in the study of De Iuliis et al. [7]. Thus, the presence of these bands indicates the presence of carbon species when synthesizing TiO_2.

To verify if carbon materials produced by the combustion of TTIP contribute to the LIE signals in our configurations, the prompt spectrum obtained at the maximum fluence (F = 0.24 J/cm^2) is compared in Fig. 7 to reference emission spectra obtained for carbon black and high-purity TiO_2 nanoparticles in a non-reactive particle dispersion system [8]. All spectra exhibit sharp emission features due to excited species of vaporized particles superimposed on a continuous curve. As expected, the emission spectrum of carbon black nanoparticles presents C_2 bands near 468 nm and 516 nm. The emission spectrum of flame-generated TiO_2 nanoparticles in this study does not show any characteristics of these emissions from carbon species. Instead, the emission spectra of flame-generated TiO_2 and high-purity TiO_2 are very similar, indicating that carbon material is likely to be in a negligible proportion. The LII signal is then originated from TiO_2 nanoparticles. Compared to previous works [7, 13], this is due to the fact that H_2 was used as fuel to stabilize the flame instead of hydrocarbons. To the best of our knowledge, this is the first time LII is applied to non-carbon-containing TiO_2. The LIE can be used to obtain an indication on the nature of the investigated particles, which has to be confirmed by ex-situ measurements such as energy-filtered transmission electron microscopy (TEM) or X-ray diffraction (XRD) [15].

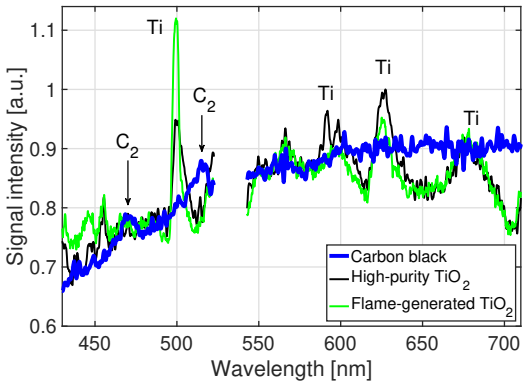

Figure 7: Emission spectra from carbon black in optical cell (blue line), high-purity TiO_2 nanoparticles in optical cell (black line) and flames-synthesized TiO_2 (at HAB= 30mm) at prompt under laser fluence of 0.24 J/cm^2 (green line).

3 Interpretation of LII signal

Once the nature of the emitted signal has been verified to have an LII-like nature and to be originated essentially from TiO_2 particles, it has to be carefully analyzed to get information on volume fraction and primary particle size.

3.1 Normalized volume fraction

Volume fraction f_v is a function of the LII signal S_{LII}, the irradiated particles effective temperature T_{eff}, the emission wavelength λ_{em}, and the absorption function $E(m_\lambda)$ as described by [16]:

$$f_v = \frac{\eta_{CAL} S_{LII}(\lambda_{em}, T_{eff}) \left[\exp\left(\frac{hc}{\lambda_{em} k_B T_{eff}}\right) - 1\right]}{\frac{12E(m_{\lambda_{em}})\pi hc^2}{\lambda_{em}^6}} \quad (1)$$

where h is the Planck constant, c the speed of light in vacuum and k_B the Boltzmann constant. η_{CAL} is a calibration factor that accounts for the effects of laser sheet thickness, detector gain, and other geometrical and spectral factors of the detection system [16].

The spatial evolution of the normalized volume fraction f_v^* can be obtained as:

$$f_v^*(z) = \frac{f_v(z)}{f_v(z_0)} \quad (2)$$

$$= \frac{S_{LII}(\lambda_{em}, T_{eff}(z))}{S_{LII}(\lambda_{em}, T_{eff}(z_0))} \frac{E(m_{\lambda_{em}}, z_0)}{E(m_{\lambda_{em}}, z)} \frac{\left[\exp\left(\frac{hc}{\lambda_{em} k_B T_{eff}(z)}\right) - 1\right]}{\left[\exp\left(\frac{hc}{\lambda_{em} k_B T_{eff}(z_0)}\right) - 1\right]} \quad (3)$$

where volume fraction $f_v(z)$ at position z has been normalized with volume fraction $f_v(z_0)$ at position z_0. To obtain information on f_v^*, it is essential to know the spatial evolution of $T_{eff}(z)$ and of $E(m_{\lambda_{em}}, z)$. To obtain information on $T_{eff}(z)$ and $E(m_{\lambda_{em}}, z)$, the spectra obtained at the prompt for flame-generated TiO_2 nanoparticles at three different flame heights and laser fluence of

F =0.15 J/cm^2 are presented in Fig. 8. The normalized curves exhibit good superposition. Assuming that the absorption function $E(m_\lambda)$ is constant along the height (z), this indicates that particles are heated by the laser at a similar effective temperature T_{eff}. Therefore, it is assumed here that $E(m_\lambda)$ and T_{eff} do not change with z. In this case, the volume fraction is then directly proportional to the LII signal.

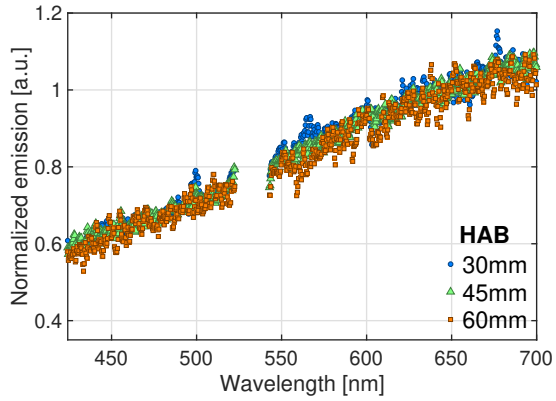

Figure 8: Emission spectra of flame-synthesized TiO_2 at different flame heights under laser fluence F = 0.15 J/cm^2. All spectra are normalized to their values at 650 nm.

The experimental 2-D spatial distribution of f_v^* along the flame height is shown in Fig. 9 by considering LII at the prompt. The laser light arrives from the left side of the image, showing the effect of certain attenuation from the left to the right side. The concentration of f_v^* is localized at the flame wings below HAB = 18 mm. For higher HABs, almost homogeneous f_v^* is observed. To our knowledge, this is the first time that the visualization of the spatial evolution of normalized volume fraction of TiO_2 nanoparticles in flames is provided using LII.

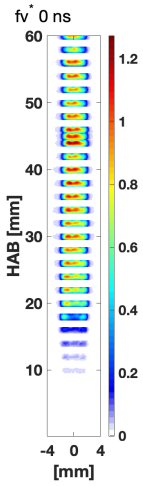

Figure 9: Spatial distribution of f_v^* assuming spatially-uniform absorption function and effective temperature.

3.2 Primary particle size

Figure 10 illustrates the normalized temporal evolution of LII measurement at 640 nm along the flame centerline for various flame heights with a laser fluence of F=0.15 J/cm^2. The LII signal decay is linked to the decay of the particle temperature during its cooling process. In general, when the particles are heated at the same peak temperature, the LII decay rate is linked to the primary particle size. In specific, the smallest the particle, the quickest it will cool down and the shorter the LII signal is. As deduced from Fig. 8, the particles are here assumed to be heated at a similar peak temperature. Thus, the decay rate of the LII signal can be processed to obtain information on primary particle size. In Fig. 10, it can be observed that the LII decay rate increases with the HABs, meaning that the primary particle size increases with the flame height.

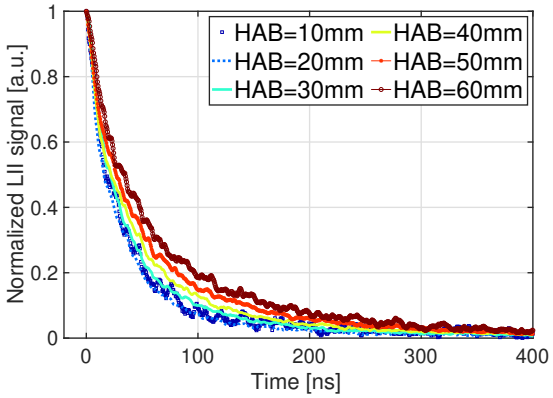

Figure 10: Normalized temporal evolution of the LII signal at 640 nm with a fluence of F = 0.15 J/cm^2 at various heights along the centerline. Each curve is normalized by its maximum value.

To illustrate this more clearly, the characteristic decay time, defined as:

$$\tau = \frac{t_i - t_j}{\ln(S_{\text{LII}}(t_j)) - \ln(S_{\text{LII}}(t_i))} \tag{4}$$

is obtained between prompt and 100 ns delayed signal for all flame heights in Fig. 11. It can be deduced that the primary particle size does not increase significantly for HAB $<$ 26 mm. Then, the primary particle size increases due to sintering or/and condensation [17]. For HAB $\geq$ 50 mm, the primary particle size is likely to reach a "plateau" value.

4 Conclusion

This study has presented the first steps towards the interpretation of the LIEs of flame-synthesized TiO_2, using an experimental set-up providing access to the spatial evolution of the spectral and temporal behavior of LIE. The results showed that the emission spectra exhibit distinctive features depending on the fluence, with the emission at longer wavelengths being attributed to incandescence for low fluence without interference from

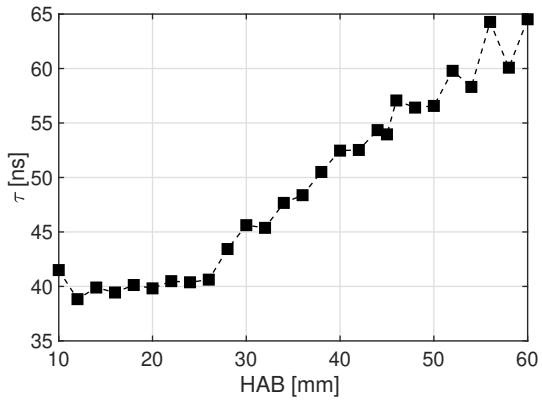

Figure 11: Variation of characteristic decay time τ of LII signal along the centerline.

the LIF/PS-LIBS signals. The optimal conditions to perform LII have been identified. The absence of carbon in the produced nanoparticles was inferred by comparing the spectral data obtained from the LIEs of flame-synthesized TiO_2 with reference spectra. LII measurements were then used to study the spatial evolution of the normalized volume fraction of particles in the flame synthesis. By analyzing the temporal evolution of LII signals, information about the primary particle size is derived. The next step in this research involves the calibration of the LII signal to obtain the volume fraction yield and quantitative primary particle size to improve our understanding of the production of flame-synthesized TiO_2.

Acknowledgments

This project has received the European Research Council (ERC) support under the European Union's Horizon 2020 research and innovation program (grant agreement No. 757912).

References

[1] W. Y. Teoh, R. Amal, and L. Mädler, Flame spray pyrolysis: An enabling technology for nanoparticles design and fabrication, *Nanoscale* **2**, 1324 (2010).

[2] H. Michelsen, C. Schulz, G. Smallwood, and S. Will, Laser-induced incandescence: Particulate diagnostics for combustion, atmospheric, and industrial applications, *Progress in Energy and Combustion Science* **51**, 2 (2015).

[3] T. A. Sipkens, J. Menser, T. Dreier, C. Schulz, G. J. Smallwood, and K. J. Daun, Laser-induced incandescence for non-soot nanoparticles: recent trends and current challenges, *Applied Physics B* **128**, 1 (2022).

[4] S. Maffi, F. Cignoli, C. Bellomunno, S. De Iuliis, and G. Zizak, Spectral effects in laser induced incandescence application to flame-made titania nanoparticles, *Spectrochimica Acta Part B: Atomic Spectroscopy* **63**, 202 (2008).

[5] F. Cignoli, C. Bellomunno, S. Maffi, and G. Zizak, Laser-induced incandescence of titania nanoparticles synthesized in a flame, *Applied Physics B* **96**, 593 (2009).

[6] S. De Iuliis, F. Migliorini, and R. Dondè, Laser-induced emission of TiO_2 nanoparticles in flame spray synthesis, *Applied Physics B* **125**, 1 (2019).

[7] S. De Iuliis, R. Dondè, and I. Altman, Light emission of flame-generated TiO_2 nanoparticles: Effect of ir laser irradiation, *Journal of Quantitative Spectroscopy and Radiative Transfer* **258**, 107353 (2021).

[8] J. Yi, C. Betrancourt, N. Darabiha, and B. Franzelli, Characterization of laser-induced emission of high-purity tio_2 nanoparticles: Feasibility of laser-induced incandescence (submitted), *Applied Physics B* (2023).

[9] G. Jellison Jr, L. Boatner, J. Budai, B.-S. Jeong, and D. Norton, Spectroscopic ellipsometry of thin film and bulk anatase (TiO_2), *Journal of Applied Physics* **93**, 9537 (2003).

[10] H.-Y. Liu, Y.-L. Hsu, H.-Y. Su, R.-C. Huang, F.-Y. Hou, G.-C. Tu, and W.-H. Liu, A comparative study of amorphous, anatase, rutile, and mixed phase TiO_2 films by mist chemical vapor deposition and ultraviolet photodetectors applications, *IEEE Sensors Journal* **18**, 4022 (2018).

[11] Sooting yale coflow diffusion flames, available at http://guilford.eng.yale.edu/yalecoflowflames/ (2016).

[12] A. Kramida, Yu. Ralchenko, J. Reader, and and NIST ASD Team, NIST Atomic Spectra Database (ver. 5.9), [Online]. Available: `https://physics.nist.gov/asd` [2022, June 2]. National Institute of Standards and Technology, Gaithersburg, MD. (2021).

[13] Y. Ren, K. Ran, S. Kruse, J. Mayer, and H. Pitsch, Flame synthesis of carbon metal-oxide nanocomposites in a counterflow burner, *Proceedings of the Combustion Institute* **38**, 1269 (2021).

[14] F. Goulay, L. Nemes, P. E. Schrader, and H. A. Michelsen, Spontaneous emission from C_2 ($d^3\Pi_g$) and C_3 ($A\,^1\Pi_u$) during laser irradiation of soot particles, *Molecular Physics* **108**, 1013 (2010).

[15] N. K. Memon, D. H. Anjum, and S. H. Chung, Multiple-diffusion flame synthesis of pure anatase and carbon-coated titanium dioxide nanoparticles, *Combustion and flame* **160**, 1848 (2013).

[16] D. R. Snelling, G. J. Smallwood, F. Liu, Ö. L. Gülder, and W. D. Bachalo, A calibration-independent laser-induced incandescence technique for soot measurement by detecting absolute light intensity, *Applied optics* **44**, 6773 (2005).

[17] B. Buesser, A. Grohn, and S. E. Pratsinis, Sintering rate and mechanism of TiO_2 nanoparticles by molecular dynamics, *The Journal of Physical Chemistry C* **115**, 11030 (2011).